Research Article | Vol. 24, No. 21 | 17 Oct 2016 | OPTICS EXPRESS 23735

Optics EXPRESS

Self-reconstruction of partially coherent light beams scattered by opaque obstacles

FEI WANG,[1,2] YAHONG CHEN,[1,2] XIANLONG LIU,[1,2] YANGJIAN CAI,[1,2,4] AND SERGEY A. PONOMARENKO[3,5]

[1]*College of physics, Optoelectronics and Energy and Collaborative Innovation Center of Suzhou Nano Science and Technology, Soochow University, Suzhou 215006, China*
[2]*Key Lab of Advanced Optical Manufacturing Technologies of Jiangsu Province and Key Lab of Modern Optical Technologies of Education Ministry of China, Soochow University, Suzhou 215006, China*
[3]*Department of Electrical and Computer Engineering, Dalhousie University, Halifax, Nova Scotia B3J2X4, Canada*
[4]*yangjiancai@suda.edu.cn*
[5]*serpo@dal.ca*

Abstract: Self-reconstruction refers to an ability of certain fully coherent optical beams to recover their spatial profiles after scattering by obstacles. In this communication, we extend the self-reconstruction concept to partially coherent beams. We show theoretically and verify experimentally that any partially coherent beam can self-reconstruct its intensity profile and state of polarization upon scattering from an opaque obstacle provided the beam coherence area is reduced well below the obstacle area. We stress that our self-reconstruction technique is independent of the obstacle shape and it is scalable to the case of multiple obstacles or even of inhomogeneous media as long as a characteristic obstacle area or a medium inhomogeneity scale is well in excess of the beam coherence area or length, respectively. We anticipate the technique to be instrumental in applications ranging from beam shaping to image transfer and trapped particle manipulation in turbid media.

OCIS codes: (030.0030) Coherence and statistical optics; (030.1640) Coherence; (110.0113) Imaging through turbid media; (350.5500) Propagation.

References and links

1. V. Garces-Chavez, D. McGloin, H. Melville, W. Sibbett and K. Dholakia, "Simultaneous micromanipulation in several planes using a self-reconstructing light beam," Nature **419**(6903), 145–147 (2002).
2. F. O. Fahrbach, P. Simon, and A. Rohrbach, "Microscopy with self-reconstructing beam," Nature Photon. **4**(11), 780–786 (2010).
3. M. McLaren, T. Mhlanga, M. J. Padgett, F. S. Roux and A. Forbes, "Self-healing of quantum entanglement after an obstruction," Nat. Commun. **5**, 3248 (2014).
4. J. Broky, G. A. Siviloglou, A. Dogariu, and D. N. Christodoulides, "Self-healing properties of optical Airy beams," Opt. Express **16**(17), 12880–12885 (2008).
5. J. Durnin, J. J. Miceli, Jr. and J. H. Eberly, "Diffraction-free beams," Phys. Rev. Lett. **58**(15), 1499–1501 (1987).
6. Z. Bouchal, "Resistance of nondiffracting vortex beams to amplitude and phase perturbations," Opt. Commun. **210**(3), 155–164 (2002).
7. S. H. Tao and X. Yuan, "Self-reconstruction property of fractional Bessel beams," J. Opt. Soc. Am. A **21**(7), 1192–1197 (2004).
8. P. Fischer, H. Little, R. L. Smith, C. Lopez-Mariscal, C. T. A. Brown, W. Sibbett and K. Dholakia, "Wavelength dependent propagation and reconstruction of white light Bessel beams," J. Opt. A **8**(5), 477–482 (2006).
9. G. A. Siviloglou, J. Broky, A. Dogariu, and D. N. Christodoulides, "Observation of accelerating Airy beams," Phys. Rev. Lett. **99**(21), 213901 (2007).
10. M. Anguiano-Morales, A. Martinez, M. D. Iturbe-Castillo, S. Chavez-Cerda, and N. Alcala-Ochoa, "Self-healing properties of a caustic optical beam," Appl. Opt. **46**(34), 8284–8290 (2007).
11. P. Vainty and P. R. Singh, "Self-healing property of optical ring lattice," Opt. Lett. **36**(15), 2994–2996 (2011).
12. J. D. Ring, J. Lindberg, A. Mourka, M. Mazilu, K. Dholakia, and M. R. Dennis, "Autofocusing and self-healing of Pearcey beams," Opt. Express **20**(17), 18955–18966 (2012).
13. S. Vyas, Y. Kozawa and S. Sato, "Self-healing of tightly focused scalar and vector Bessel-Gauss beams at the focal plane," J. Opt. Soc. Am. A **28**(5), 837–843 (2011).

#274499 http://dx.doi.org/10.1364/OE.24.023735
Journal © 2016 Received 25 Aug 2016; revised 26 Sep 2016; accepted 27 Sep 2016; published 3 Oct 2016

Optics EXPRESS

14. G. Wu, F. Wang, and Y. Cai, "Generation and self-healing of a radially polarized Bessel-Gauss beam," Phys. Rev. A **89**(4), 043807 (2014).
15. L. Mandel and E. Wolf, *Optical Coherence and Quantum Optics* (Cambridge University, 1995).
16. Y. Chen, J. Gu, F. Wang, and Y. Cai, "Self-splitting properties of a Hermite-Gaussian correlated Schell-model beam," Phys. Rev A **91**(1), 013823 (2015).
17. S. Sahin and O. Korotkova, "Light sources generating far fields with tunable flat profiles," Opt. Lett. **37**(14), 2970–2972 (2012).
18. Y. Chen, F. Wang, L. Liu, C. Zhao, Y. Cai, and O. Korotkova, "Generation and propagation of a partially coherent vector beam with special correlation functions," Phys. Rev. A **89**(1), 013801 (2014).
19. L. Ma and S. A. Ponomarenko, "Optical coherence gratings and lattices," Opt. Lett. **39**(23), 6656–6660 (2014).
20. L. Ma and S. A. Ponomarenko, "Free-space propagation of optical coherence lattices," Opt. Express **23**(2), 1848–1856 (2015).
21. D. Paganin, and K. A. Nugent, "Noninterferometric phase imaging with partially coherent light," Phys. Rev. Lett. **80**(12), 2586–2589 (1998).
22. L. W. Whitehead, G. J. Williams, H. M. Quiney, D. J. Vine, R. A. Dilanian, S. Flewett, and K. A. Nugent, "Diffractive imaging using partially coherent X-rays," Phys. Rev. Lett. **103**(24), 243902 (2009).
23. J. N. Clark, X. Huang, R. Harder and I. K. Robinson, "High-resolution three-dimensional partially coherent diffraction imaging," Nat. Commun. **3**, 993 (2012).
24. A. Valencia, G. Scarcelli, M. D'Angelo, and Y. Shih, "Two-photon imaging with thermal light," Phys. Rev. Lett. **94**(6), 063601 (2005).
25. P. Ryczkowski, M. Barbier, A. T. Friberg, J. M. Dudley and G. Genty, "Ghost imaging in the time domain," Nature Photon. **10**(3), 167–170 (2016).
26. M. Takeda, W. Wang, Z. Duan, and Y. Miyamoto, "Coherence holography," Opt. Express **13**(23), 9629–9635 (2005).
27. S. Divitt, and L. Novotny, "Spatial coherence of sunlight and its implications for light management in photovoltaics," Optica **2**(2), 95–103 (2015)
28. M. Mitchell, Z. Chen, M. Shih, and M. Segev, "Self-trapping of partially spatially incoherent light," Phys. Rev. Lett. **77**(3), 490–493 (1996).
29. M. Mitchell, and M. Segev, "Self-trapping of incoherent white light," Nature **387**(6636), 880–882 (1997).
30. C. C. Jeng, M. F. Shih, K. Motzek, and Y. Kivshar, "Partially incoherent optical vortices in self-focusing nonlinear media," Phys. Rev. Lett. **94**(4), 043904 (2004).
31. L. Waller, G. Situ, and J. Fleischer, "Phase-space measurement and coherence synthesis of optical beams," Nature Photon. **6**(7), 474–479 (2012).
32. R. Carminati and J. J. Greffet, "Near-field effects in spatial coherence of thermal sources," Phys. Rev. Lett. **82**(8), 1660–1663 (1999).
33. H. Roychowdhury and E. Wolf, "Effects of spatial coherence on near-field spectra," Opt. Lett. **28**(3), 170–172 (2003).
34. A. Apostol and A. Dogariu, "Spatial correlations in the near field of random media," Phys. Rev. Lett. **91**(9), 093901 (2003).
35. C. H. Gan, Y. Gu, T.D. Visser and G. Gbur, "Coherence converting plasmonic hole arrays," Plasmonics **7**(2), 313–322 (2012).
36. T. Saastamoinen and H. Lajunen, "Increase of spatial coherence by subwavelength metallic gratings," Opt. Lett. **38**(23), 5000–5003 (2013).
37. A. Aiello and J. P. Woerdeman, "Physical bounds to the entropy-depolarization relation in random light scattering," Phys. Rev. Lett. **94**(9), 090406 (2005).
38. T. Yarnall, A. F. Abourrady, B. E. A. Saleh, and M. C. Teich, "Spatial coherence effects in second-and fourth-order temporal interference," Opt. Express **16**(11), 7634–7640 (2008).
39. B. N. Simon, S. Simon, F. Gori, M. Santarsiero, R. Borghi, N. Mukunda, and R. Simon, "Nonquantum entanglement resolves a basic issue in polarization optics," Phys. Rev. Lett. **104**(2), 023901 (2010).
40. K. H. Kagalwala, G. D. Guiseppe, A. F. Abouraddy, and B. E. A. Saleh, "Bell's measure in classical optical coherence," Nature Photon. **7**(1), 72–78 (2013).
41. X. F. Qian, B. Little, J. C. Howell, and J. H. Eberly, "Shifting the quantum-classical boundary: theory and experiment for statistically classical optical fields," Optica **2**(7), 611–615 (2015).
42. J. W. Goodman, *Statistical Optics*, 2nd Ed., (Wiley, New York, 2015).
43. J. W. Goodman, *Introduction to Fourier Optics*, 2nd Ed., (McGraw-Hill, 1998).
44. E. Wolf, *Introduction to the Theory of Coherence and Polarization of Light* (Cambridge University, 2007).
45. Z. Hradil, J. Rehacek, and L. L. Sanchez-Soto, "Quantum reconstruction of the mutual coherence function," Phys. Rev. Lett. **105**(1), 010401 (2010).
46. B. Stoklasa, L. Motka, J. Rehacek, Z. Hradil, and L. L. Sanchez-Soto, "Wavefront sensing reveals optical coherence," Nat. Commun. **5**, 3275 (2014).
47. S. A. Ponomarenko, "Self-imaging with partially coherent light in graded-index media," Opt. Lett. **40**(4), 566–568 (2015).

Optics EXPRESS

1. Introduction

It has been known for some time that whenever certain types of fully coherent light beams encounter an obstacle, either in free space or in inhomogeneous media, they are able to reconstitute their spatial shape upon interaction with the obstacle. Optical self-reconstruction has already found applications to microscopic particle manipulation [1], human tissue microscopy [2], quantum entanglement propagation in the presence of obstructions [3] and optical communications through inhomogeneous media [4] among others and it has even inspired science fiction writers.

This self-reconstruction property has first emerged as a signature of diffraction-free beams such as fundamental [5], higher-order vortex [6], fractional [7] and white-light [8] Bessel beams as well as Airy [4, 9] and caustic [10] beams. It was subsequently shown that even some diffracting coherent beams, including optical ring lattices [11], Pearcey beams [12], tightly focused [13] and radially polarized [14] Bessel-Gauss beams, can self-reconstruct. However, the self-reconstruction power of all fully coherent self-healing light beams known to date hinges on engineering special beam profiles and in many cases, it is sensitive to the obstacle size, shape and distribution, thereby limiting applications of such beams.

Partially coherent beams are distinguished by the profound dependence of their spatial profile, polarization, propagation through and interaction with material media on beam coherence properties [15]. In particular, spatial coherence has proven to be a fundamental degree of freedom, indispensable for controlled generation of partially coherent beams with novel properties such as self-splitting [16], flat-top intensity profile [17], radial polarization [18] as well as far-field optical lattice patterns [19, 20], tailored to desired applications, including non-interferometric phase imaging [21], diffractive imaging [22, 23], ghost imaging [24, 25], coherence holography [26], and photovoltaics [27]. The exploration of spatial coherence degree of freedom has also expanded research horizons in nonlinear optics [28–31] and near-field optics [32–36]. Furthermore, optical coherence has emerged as one of the key subjects in recent studies of analogies between quantum and classical entanglement [37–41], and it is anticipated to play a major role in delineating an elusive boundary between classical and quantum realms. The fundamental importance of spatial coherence in classical and quantum physics and the prominent role played by optical self-reconstruction in many promising applications prompt an intriguing question: Can one manipulate spatial coherence of a light source to ensure self-reconstruction of arbitrarily shaped generated beams, scattered by an obstruction or by an inhomogeneous medium, either deterministic or random?

We address this challenge here by introducing a novel self-reconstruction protocol applicable to any nearly incoherent optical beam regardless of its intensity profile and polarization state particulars. We show both theoretically and experimentally that making the spatial coherence area of any optical beam much smaller than the obstacle area is a key prerequisite to successful self-reconstruction of the beam intensity and polarization distributions.

2. Qualitative picture of nearly incoherent beam self-reconstruction

To gain insight into the new protocol, we first consider qualitatively the scattering of a nearly incoherent beam of diameter σ_I and a characteristic coherence length σ_c by a circular aperture of diameter σ_a serving as an isolated obstacle. We assume that $\sigma_c \ll \sigma_a < \sigma_I$. The situation is illustrated in Fig.1. The nearly incoherent beam, which is known to be composed of a number of randomly distributed uncorrelated beamlets of the size $\sigma_c \ll \sigma_I$ [15], has a diffraction angular spread $\theta_d \sim \lambda/\sigma_c$, entirely determined by the beam wavelength λ and its coherence length σ_c . This is because each beamlet behaves as a fully coherent structure of the size equal to the overall beam coherence length. Since the obstacle causes the scattering angular spread of $\theta_s \sim \lambda/\sigma_a \ll \theta_d$, the nearly incoherent beam is relatively impervious to the obstacle and is able to self-reconstruct its intensity profile and polarization state upon scattering from it.

Optics EXPRESS

The presented self-reconstruction principle can be naturally extended to the case of multiple obstructions such that the smaller of a characteristic obstacle scale or an inter-obstacle distance is still much greater than the incident beam coherence length. In case of a continuous inhomogeneous medium, the present self-reconstruction scenario can work out provided a characteristic refractive index inhomogeneity scale of the medium dwarfs the beam coherence length.

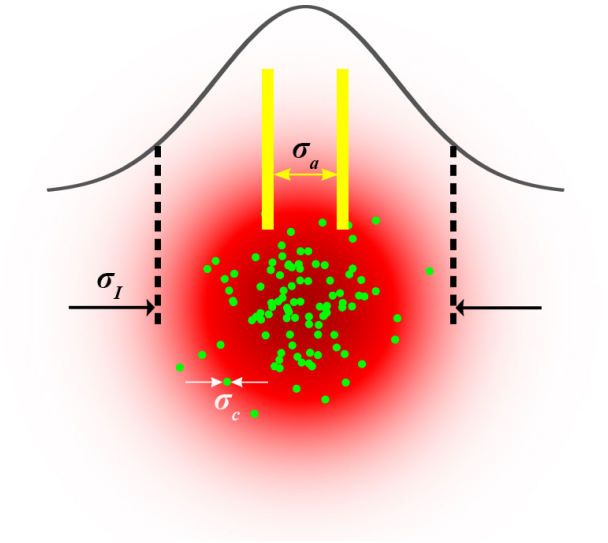

Fig. 1. Qualitative illustration of nearly incoherent beam scattering by an obstacle. Nearly incoherent beam of diameter σ_I and coherence length σ_c has a specular structure with each speckle beamlet having the spot size equal to the beam coherence length. The obstacle is modeled by a circular aperture of width σ_a .

The outlined self-reconstruction principle is clearly independent of the obstacle shape and the necessary condition for beam self-reconstruction can be formulated in terms of the beam coherence area A_c, the obstacle area A_a and the beam intensity cross-section area A_I as

$$A_c \ll A_a < A_I. \tag{1}$$

We stress here a fundamental difference of fully from that of partially coherent beam self-reconstruction. While the former relies on special properties of diffraction-free complex amplitude profiles, the latter is ensured by judicial beam coherence engineering.

3. Theoretical formulation and numerical self-reconstruction

To confirm quantitatively the just described qualitative picture of partially coherent beam self-reconstruction, we introduce the cross-spectral density tensor of the electromagnetic field **E** ensemble, describing random beams in the source plane $z = 0$, as [15]

$$W_{ij}{}^{(0)}(\rho_1, \rho_2) = \langle E_i^*(\rho_1) E_j(\rho_2) \rangle, \tag{2}$$

Here $i, j = x, y; \rho$ is a position vector in the plane transverse to the beam propagation direction, and the angle brackets denote statistical ensemble averaging. We specifically consider the input beam of a Schell-model type such that

$$W_{ij}^{(0)}(\rho_1, \rho_2) = \sqrt{I_i(\rho_1) I_j(\rho_2)}\, g_{ij}(\rho_1 - \rho_2), \tag{3}$$

Optics EXPRESS

where $I_{i,j}$ stand for intensity components along the x, y-axes and $g_{i,j}$ describes (statistically homogeneous) second-order field correlations. A Schell-model beam can be readily generated by transmitting an arbitrary coherent beam through a rotating ground-glass disk [32]. The transmitted beam coherence length can be controlled by adjusting the disk rotation speed and the incident beam spot size at the ground-glass disk.

Next, we place an obstacle illuminated by the Schell-model beam in the focal plane behind a thin lens with the focal length $f = 250mm$ (source plane) and examine the scattered beam image in the focal plane in front of the lens (image plane). The lens performs a Fourier transform of the scattered partially coherent beam cross-spectral density tensor [33] (see Appendix A). The intensity and polarization state of the scattered beam can be inferred from the Stokes parameters defined as [34]

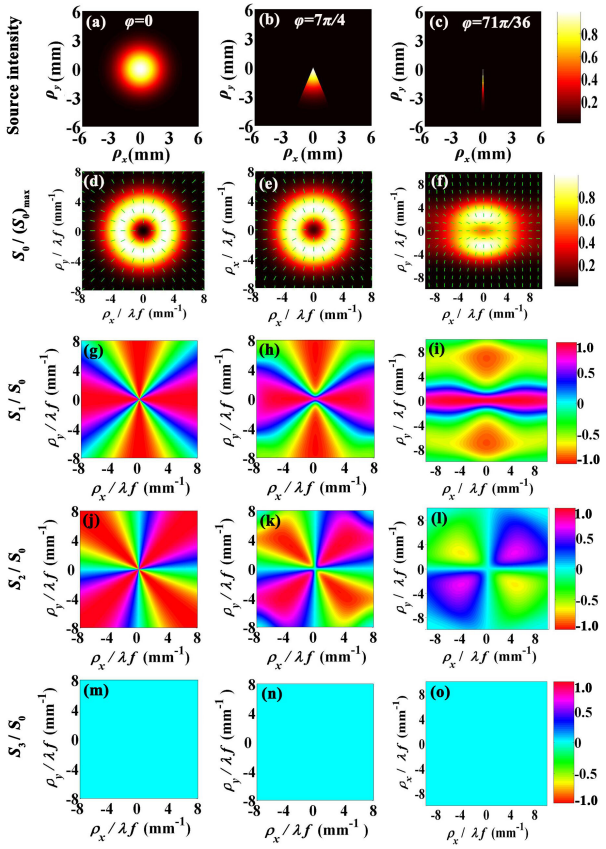

Fig. 2. Numerical self-reconstruction of a radially polarized Schell-model beam scattered by a sector-shaped opaque object (SSOO). Intensity and Stokes' parameter distribution of the beam in the source plane and in the image plane with no obstruction (left column) and with the SSOO with the angle $\varphi = 7\pi/4$ (middle column) and $\varphi = 71\pi/36$ (right column). The beam parameters are: $\sigma_I = 1.5mm$ and $\sigma_c = 75\mu m$ and the SSOO has the same diameter as the beam, $\sigma_a = \sigma_I$.

$$S_0(\rho) = W_{xx}(\rho,\rho) + W_{yy}(\rho,\rho), \tag{4}$$

$$S_1(\rho) = W_{xx}(\rho,\rho) - W_{yy}(\rho,\rho), \tag{5}$$

$$S_2(\rho) = W_{xy}(\rho,\rho) + W_{yx}(\rho,\rho), \tag{6}$$

Optics EXPRESS

$$S_3(\rho) = i(W_{yx}(\rho,\rho) - W_{xy}(\rho,\rho)), \tag{7}$$

here $S_0(\rho)$ represents the average beam intensity.

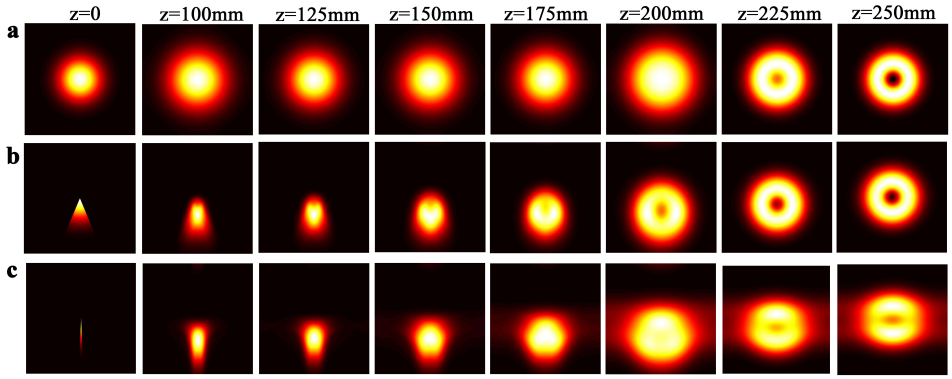

Fig. 3. Numerical transient dynamics of the RPSM beam scattered by a sector-shaped opaque object (SSOO) at several distances. **a** Intensity distribution of the beam at several propagation distance without obstructed. **b** Intensity distribution of the beam at several propagation distance with the SSOO center angle $\varphi = 7\pi/4$ and **c** with the SSOO center angle $\varphi = 71\pi/36$. The beam parameters are the same as Fig. 2.

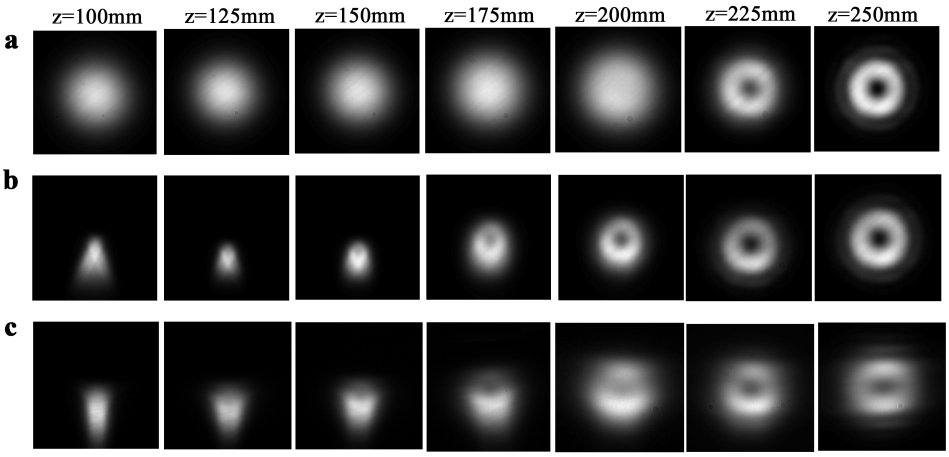

Fig. 4. Experimental transient dynamics of the RPSM beam scattered by a sector-shaped opaque object (SSOO) at several distances. **a** Intensity distribution of the beam at several propagation distance without obstructed. **b** Intensity distribution of the beam at several propagation distance with the SSOO center angle $\varphi = 7\pi/4$ and **c** with the SSOO center angle $\varphi = 71\pi/36$. The beam parameters are the same as Fig. 2.

As a numerical example, we studied the scattering of a radially polarized Schell-model (RPSM) beam introduced in [18] (see Appendix A for beam structure details) with the beam width $\sigma_I = 1.5mm$ and coherence length $\sigma_c = 75\mu m$ by a sector-shaped opaque object (SSOO) with a center angle φ and diameter $\sigma_a = 1.5mm$. We exhibit the simulation results in Fig.2. The left column, Figs. 2(a), 2(d), 2(g), 2(j), and 2(m), shows the unobstructed beam intensity in the source plane and in the image plane and polarization distributions in the image plane,

Optics EXPRESS

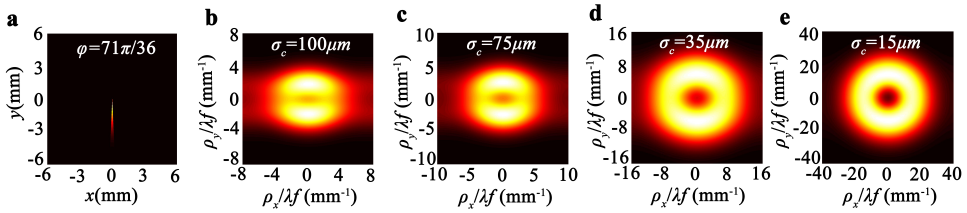

Fig. 5. Numerical self-reconstruction ability of a RPSM beam scattered by a SSOO. **a** Intensity distribution of the beam in the source plane with SSOO center angle $\varphi = 71\pi/36$. **b, c, d** and **e** Intensity distribution of the beam in the focal plane with different coherence length σ_c .

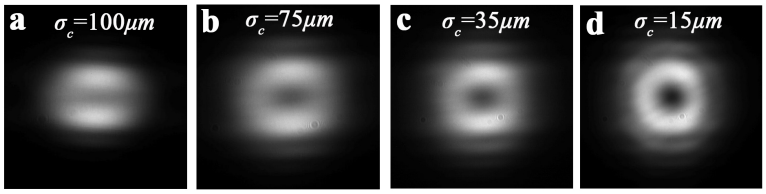

Fig. 6. Experimental self-reconstruction ability of a RPSM beam scattered by a SSOO with center angle $\varphi = 71\pi/36$. **a, b, c,** and **d** Intensity distribution of the beam in the focal plane with different coherence length σ_c .

respectively, while the middle one, Figs. 2(b), 2(e), 2(h), 2(k), and 2(n), demonstrates the beam self-reconstruction in the presence of the SSOO blocking most of the input beam cross-section. The SSOO area conforms to the constraint set by Eq.(1). We also show in the right column of Fig. 2 that as the SSOO transmittance area approaches the beam coherence area, violating the conditions of Eq.(1), the beam self-reconstruction ability is severely inhibited.

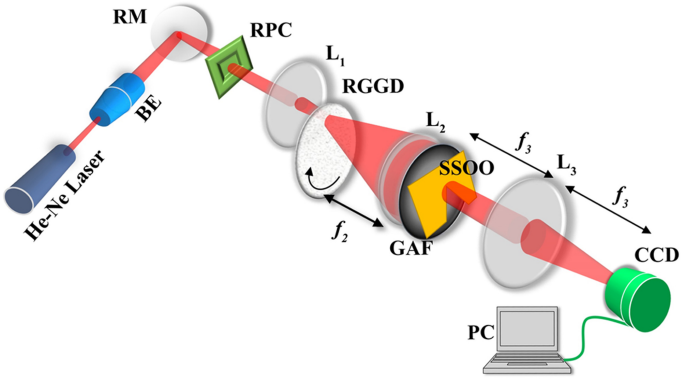

Fig. 7. Experimental setup for RPSM beam self-reconstruction demonstration. Beam expander (BE), reflecting mirror; (RM), radial polarization converter (RPC), rotating ground-glass disk (RGGD); L_1, L_2, L_3, thin lenses, Gaussian amplitude filter (GAF), sector-shaped opaque obstacle (SSOO), charge-coupled device (CCD).

We note that (nearly perfect) self-reconstruction of the beam is realized in the image plane of the lens. There are some distortions caused by the obstacle immediately after scattering and on propagation to the image plane. We exhibit the RPSM beam transient dynamics at several

Optics EXPRESS

distances behind the image plane in Figs. 3 and 4, and its self-reconstruction ability in Figs. 5 and 6.

4. Experimental results

4.1. Case I: Single obstacle

We carried out experimental self-reconstruction of an RPSM beam upon its scattering from a single sector-shaped opaque object. The RPSM beam and the imaging lens had the same parameters as in our numerical simulations. The experimental setup, sketched in Fig. 7, was identical with that in [18] (see Appendix B for particulars) except the SSOO, placed in the focal plane of lens L_3, was present. In particular, a fully coherent beam, generated by a He-Ne laser was transmitted through a beam expander (BE) and having been reflected by a reflecting mirror (RM), the beam passed through a radial polarization converter (RPC). We then converted a fully coherent radially polarized beam into the RPSM by transmitting the former through a rotating ground-glass disk (RGGD) and Gaussian amplitude filter (GAF). The resulting RPSM beam was scattered by an SSOO with the variable center angle φ, placed in the source plane of the lens L_3, optically Fourier transformed into the lens image plane and registered by a charge-coupled device (CCD).

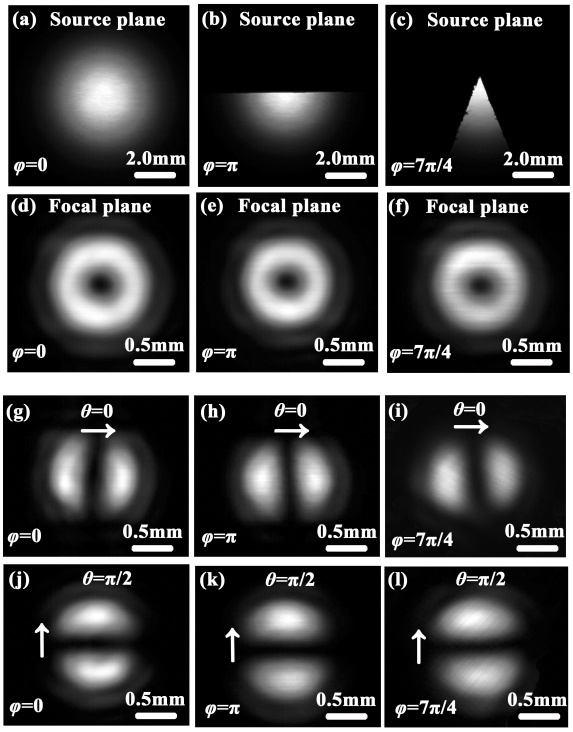

Fig. 8. Experimental beam self-reconstruction: Case 1. SSOO. Left column: Intensity and polarization distributions of the RPSM beam in the source and focal planes in the absence of obstruction. Middle column: The same as in the left column, except the SSOO blocking half of the beam cross-section is placed in the source plane. Right column: Same as the middle one with the SSOO having the center angle $\varphi = 7\pi/4$. The linearly polarized-with an inserted linear polarizer not shown in Fig. 3-imaged beam has the polarization direction indicated by the arrow. The beam polarization direction makes the angle θ with the x-axis.

Optics EXPRESS

We display the experimental results in Fig. 8 where the left column shows the unobstructed RPSM beam intensity and polarization distributions in the source and image planes. In the middle column, we display the same quantities when the beam is scattered by the SSOO that covers half the cross-section area of the RPSM beam in the source plane. The accurate beam intensity profile and the polarization state recovery is evident from the figure. The right column of the figure exhibits high-quality self-reconstruction of the beam subject to the SSOO obstructing the greater part of the beam cross-section. The RPSM beam is linearly polarized with the polarization direction making the angle θ with the x-axis. The RPSM beam polarization direction in the image plane is indicated by the arrow.

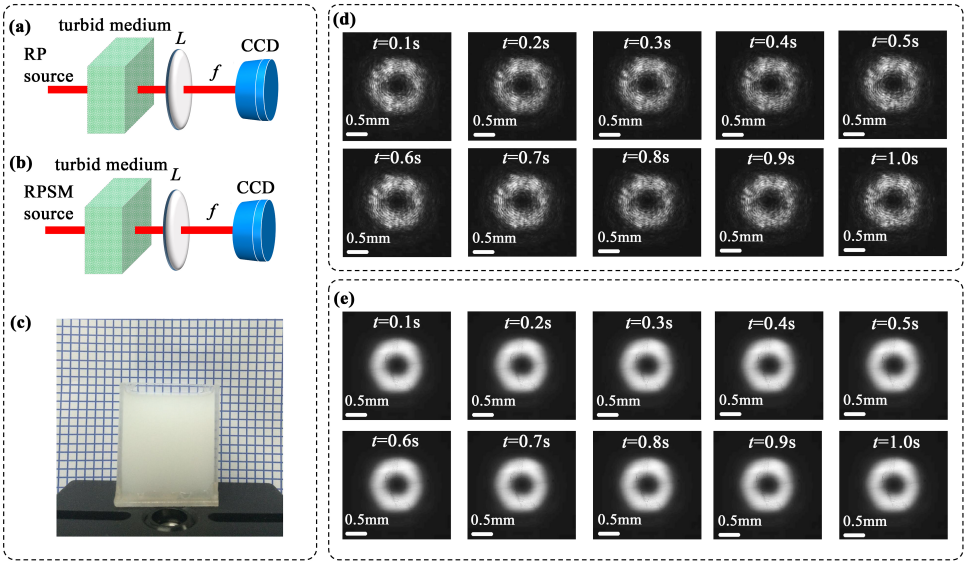

Fig. 9. Experimental beam self-reconstruction: case 2. Turbid medium. (a) Experimental setup for analyzing fully coherent radially polarized beam transmission through a turbid medium with random refractive index fluctuations. (b) Experimental setup for analyzing the RPSM beam transmission through the same turbid medium. (c) Photograph of the turbid medium (diluted milk). (d) Experimental intensity profile self-reconstruction of the fully coherent radially polarized beam passing through diluted milk at different instances of time t. (see also Visualization 1) (e) Experimental intensity profile self-reconstruction of the RPSM beam passing through diluted milk at different time instances t. (see Visualization 2 as well).

4.2. *Case II: Scattering by turbid medium*

We also examined self-reconstruction of the RPSM beam transmitted through a colloidal medium. A glass of diluted milk, shown in Fig. 9 (c), served as the scattering medium in our experiments. The medium can be viewed as random because the colloidal particle density fluctuations in the milk lead to the refractive index fluctuations. The latter cause scattering of the light transmitted through the glass. In Figs. 9 (a) and 9(b) we display schematics of the experimental setup for the cases of fully coherent radially polarized and RPSM beams, respectively. The RPSM beam coherence length and beam width were taken to be $\sigma_c = 75\mu m$ and $\sigma_I = 1.5mm$, respectively. The beam width of fully coherent RP beam was taken to be $\sigma_I = 350\mu m$ to make sure that the beam size in the detect plane was nearly same with that of the focusing RPSM beam in the detect plane. Each beam was transmitted through the glass of milk and then focused by a thin lens L with the focal length $f = 250mm$ onto the CCD camera located in the image plane of the lens. In

Optics EXPRESS

Figs. 9(d) and 9(e) we exhibit the experimental results of the intensity profile of the transmitted radially polarized coherent beam and that of the RPSM beam at different time instances. We can clearly detect the difference in the quality of self-reconstructed images. While the coherent transmitted beam is strongly affected by the medium resulting in poor self-reconstruction with a granular structure, the transmitted RPSM beam is seen to possess a smooth spatial intensity distribution, reproducing well the RPSM beam in the image plane.

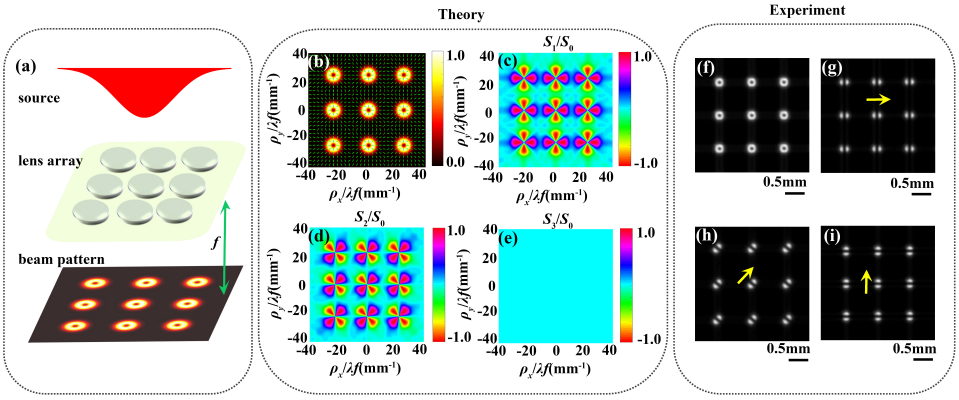

Fig. 10. Radially polarized beam array generation through the RPSM source self-reconstruction. (a) Schematics of the apparatus for generation of a radially polarized beam array. (b) Numerical simulation results of the generated beam array intensity profile and the state of polarization. Both the diameter of each lens and the distance between the centers of adjacent lenses are 1mm. The focal length of the lens array is 65.6*mm*. (c), (d), (e) Stokes' parameter distributions of the radially polarized beam array; (f), (g), (h), (i) experimental results of the generated radially polarized beam array intensity and the state of polarization. The arrow indicates the polarization direction of the beam.

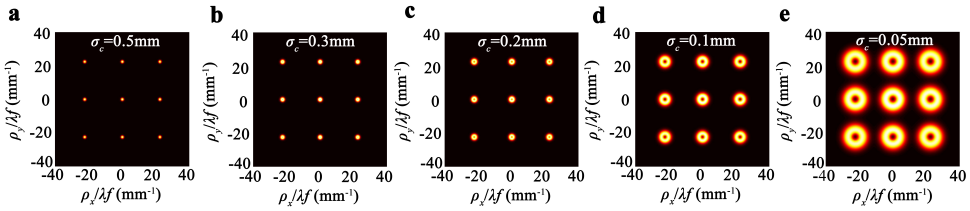

Fig. 11. Numerical formation of radial polarized beam array as a function of the input beam coherence. **a-e** Numerical simulation results of the generated beam array intensity profile with difference beam coherence.

5. Promising applications and summary

Apart from the image and/or information transfer and optical communications through adverse inhomogeneous environments, the proposed self-reconstruction protocol can be useful for generating novel types of partially coherent sources, inaccessible in the realm of coherent optics. The latter property stems from the inherent ability of sources with controlled spatial coherence to self-reconstruct whenever the source cross-section area is partially obstructed by an obstacle provided the source coherence area is engineered to be much smaller than the obstructed source

Optics EXPRESS

area. This opens up an exciting possibility for realizing periodic arrays of partially coherent beams with prescribed spatial intensity profile and state of polarization in the focal plane of a lens by focusing vector partially coherent beams with lens arrays. As an illustrative example, we consider focusing of an RPSM beam with the same parameters as in the previous sections by a 3×3 thin lens array with the focal length $f = 65.6mm$. The schematic of the experiment is shown in Fig. 10(a). Both the diameter of each lens and the distance between the centers of adjacent lenses were taken to be $1mm$. Due to the RPSM beam self-reconstruction upon scattering by each individual lens aperture, the transmitted field from each lens forms an annular beam spot with radial polarization in the focal plane of the lens. Consequently, a 3×3 radially polarized beam array is formed in the focal plane. In Figs. 10(b)-10(e), we display our simulation results while Figs. 10 (f)-10(i) show an experimentally generated radially polarized beam array. To emphasize the spatial coherence role in the microlens array formation, we show how the array forms as a function of the input beam coherence in Fig. 11 and in Visualization 3. We anticipate these microlens arrays to find applications for multiple particle trapping and manipulations. Next, thereby synthesized microlens arrays can be used in conjunction with the Shack-Hartmann wavefront sensing protocol to determine the coherence state of a test source beam via the wavefront sensing [45,46]. Furthermore, we point out an attractive extension of our protocol to the case of disordered self-focusing nonlinear media. The self-focusing nonlinearities in such media will oppose rapid diffraction of low-coherence self-reconstructed beams and open up an opportunity to transmit the input beam images over longer distances than it is possible in random linear media. Finally, the present self-reconstruction should be distinguished from partially coherent beam self-imaging that only occurs at certain distances within graded-index media [47].

In summary, we have shown that any partially coherent beam, scattered by an arbitrary opaque obstacle, can recover its intensity profile and the state of polarization provided the spatial coherence area of the beam is made much smaller than the obstacle area. The presented self-reconstruction technique is scalable to the case of multiple obstacles with a characteristic inter-obstacle distance being much greater than the obstacle size. The technique also extends to scattering in inhomogeneous media, either deterministic or random, with a characteristic inhomogeneity scale dwarfing the beam coherence length.

Appendix A. Numerical simulations

In our numerical simulations and experimental demonstration of self-reconstruction, we employ radially polarized Schell-model (RPSM) beam which was introduced and studied in detail in [18]. Our RPSM beams have Gaussian intensity profiles with the same width $\sigma_I = 1.5mm$ along each Cartesian axis and the two-point correlation tensor g_{ij} with the diagonal and off-diagonal components in the form

$$g_{aa}(\rho_1, \rho_2) = \left[1 - \frac{(a_1 - a_2)^2}{\sigma_c^2}\right] \exp\left[-\frac{(\rho_1 - \rho_2)^2}{2\sigma_c^2}\right] \tag{8}$$

where $a = x, y$ and

$$g_{xy}(\rho_1, \rho_2) = g_{yx}(\rho_1, \rho_2) = -\frac{(x_1 - x_2)(y_1 - y_2)}{\sigma_c^2} \exp\left[-\frac{(\rho_1 - \rho_2)^2}{2\sigma_c^2}\right], \tag{9}$$

respectively. The correlation length is $\sigma_c = 75\mu m$.

The opaque obstacle is modeled by a generic transmittance amplitude $T(\rho)$ such that

$$T(\rho) = \{1 \text{ transmission region}, 0 \text{opaque region}. \tag{10}$$

The cross-spectral density tensor of the RPSM beam immediately behind the obstacle reads

$$W_{ij}^{(sc)}(\rho_1, \rho_2) = T(\rho_1) T(\rho_2) \sqrt{I(\rho_1) I(\rho_2)} g_{ij}(\rho_1 - \rho_2). \tag{11}$$

Optics EXPRESS

An imaging lens with the focal lens $f = 250mm$ transforms the scattered RPSM beam, placed in its focus, into an image in the focal plane in the front of the lens. Thus, the lens performs a Fourier transformation of the scattered cross-spectral density tensor yielding

$$W_{ij}(\rho_1, \rho_2) = \frac{1}{\lambda^2 f^2} \widetilde{W}_{ij}^{(sc)}(\rho_1/\lambda f, \rho_2/\lambda f), \tag{12}$$

where tilde denotes a Fourier transform. Using Eqs. (10)-(12) as well as the Stokes parameter definitions, Eqs. (4) to (7) in the main text, we can determine the intensity and polarization distribution of the imaged RPSM beams.

Appendix B. Experimental realization

The $632.991nm$ carrier wavelength He-Ne Laser used in our experiment is fabricated by Thorlabs, Inc. (HRS015B). The beam expander is manufactured by Daheng Optics, Inc. (GCO-2501). It has an operating wavelength of $450nm$ to $680nm$, and expanding ratio of 5 to 10. The radial polarization converter is used to convert the linear polarization to radial polarization (RADPOL4, Arcoptix). The surface roughness of ground-glass disc is 400 mesh number and the rotating speed is 3000r/min. The CCD camera is acquired from Point Grey, Inc. (GRAS-20S4M-C) with its resolution of 1624×1224, and Frame Rate, 30 FPS. The integration time of CCD camera during optimization was $20ms$ and the Frame rate was set to 10 FPS for video. The 3×3 lens array (APO-Q-P1000-R30) is acquired from Advanced Mirooptic Systems Gmbh and its focal length $f = 65.6mm$. Both the diameter of each lens and the distance between the centers of adjacent lenses are $1mm$.

Funding

National Natural Science Fund for Distinguished Young Scholar (11525418); National Natural Science Foundation of China (11274005, 11474213); Project of the Priority Academic Program Development (PAPD) of Jiangsu Higher Education Institutions; National Science and Engineering Research Council of Canada (NSERC);Innovation Plan for Graduate Students in the Universities of Jiangsu Province (KYZZ16_0079).